Search for the $K_S \to e^+e^-$ decay with the *KLOE* detector at *DAΦNE*

The KLOE Collaboration

F. Ambrosino [d], A. Antonelli [a], M. Antonelli [a], F. Archilli [a,1],
C. Bacci [h], P. Beltrame [b], G. Bencivenni [a], S. Bertolucci [a],
C. Bini [g], C. Bloise [a], S. Bocchetta [h], V. Bocci [g], F. Bossi [a],
P. Branchini [h], R. Caloi [g], P. Campana [a], G. Capon [a],
T. Capussela [d], F. Ceradini [h], S. Chi [a], G. Chiefari [d],
P. Ciambrone [a], E. De Lucia [a], A. De Santis [g], P. De Simone [a],
G. De Zorzi [g], A. Denig [b], A. Di Domenico [g], C. Di Donato [d],
S. Di Falco [e], B. Di Micco [h], A. Doria [d], M. Dreucci [a], G. Felici [a],
A. Ferrari [a], M. L. Ferrer [a], G. Finocchiaro [a], S. Fiore [g],
C. Forti [a], P. Franzini [g], C. Gatti [a], P. Gauzzi [g], S. Giovannella [a],
E. Gorini [c], E. Graziani [h], M. Incagli [e], W. Kluge [b], V. Kulikov [k],
F. Lacava [g], G. Lanfranchi [a], J. Lee-Franzini [a,i], D. Leone [b],
M. Martini [a], P. Massarotti [d], W. Mei [a], S. Meola [d], S. Miscetti [a],
M. Moulson [a], S. Müller [a], F. Murtas [a], M. Napolitano [d],
F. Nguyen [h], M. Palutan [a,2], E. Pasqualucci [g], A. Passeri [h],
V. Patera [a,f], F. Perfetto [d], M. Primavera [c], P. Santangelo [a],
G. Saracino [d], B. Sciascia [a], A. Sciubba [a,f], F. Scuri [e], I. Sfiligoi [a],
T. Spadaro [a,3], M. Testa [g], L. Tortora [h], P. Valente [g],
B. Valeriani [b], G. Venanzoni [a], R.Versaci [a], G. Xu [a,j]

[a]*Laboratori Nazionali di Frascati dell'INFN, Frascati, Italy.*

[b]*Institut für Experimentelle Kernphysik, Universität Karlsruhe, Germany.*

[c]*Dipartimento di Fisica dell'Università e Sezione INFN, Lecce, Italy.*

[d]*Dipartimento di Scienze Fisiche dell'Università "Federico II" e Sezione INFN, Napoli, Italy*

[e]*Dipartimento di Fisica dell'Università e Sezione INFN, Pisa, Italy.*

[f]*Dipartimento di Energetica dell'Università "La Sapienza", Roma, Italy.*

[g]*Dipartimento di Fisica dell'Università "La Sapienza" e Sezione INFN, Roma, Italy.*

[h]*Dipartimento di Fisica dell'Università "Roma Tre" e Sezione INFN, Roma, Italy.*

arXiv:0707.2687v1 [hep-ex] 18 Jul 2007

[i]*Physics Department, State University of New York at Stony Brook, USA.*

[j]*Permanent address: Institute of High Energy Physics of Academica Sinica, Beijing, China.*

[k]*Permanent address: Institute for Theoretical and Experimental Physics, Moscow, Russia.*

Abstract

We present results of a direct search for the decay $K_S \to e^+e^-$ with the KLOE detector, obtained with a sample of $e^+e^- \to \phi \to K_S K_L$ events produced at DAΦNE, the Frascati ϕ–factory, for an integrated luminosity of 1.3 fb^{-1}. The Standard Model prediction for this decay is BR$(K_S \to e^+e^-) = 1.6 \times 10^{-15}$. The search has been performed tagging the K_S decays by simultaneous detection of a K_L interaction in the calorimeter. Background rejection has been optimized by using both kinematic cuts and particle identification. At the end of the analysis chain we find BR$(K_S \to e^+e^-) < 2.1 \times 10^{-8}$ at 90% CL, which improves by a factor of ~ 7 on the previous best result, obtained by CPLEAR experiment.

1 Introduction

The decay $K_S \to e^+e^-$, like the decay $K_L \to e^+e^-$ or $K_L \to \mu^+\mu^-$, is a flavour-changing neutral-current process, suppressed in the Standard Model and dominated by the two-photon intermediate state [1]. For both K_S and K_L, the e^+e^- channel is much more suppressed than the $\mu^+\mu^-$ one (by a factor of ~ 250) because of the $e - \mu$ mass difference. The diagram corresponding to the process $K_S \to \gamma^*\gamma^* \to \ell^+\ell^-$ is shown in Fig. 1. Using Chiral Perturbation
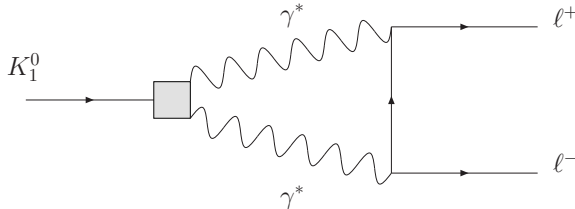

Fig. 1. Long distance contribution to $K_S \to \ell^+\ell^-$ process, mediated by two-photon exchange.

Theory (χpT) to order $\mathcal{O}(p^4)$, G. Ecker and A. Pich evaluated the ratio [1] $\Gamma(K_S \to e^+e^-)/\Gamma(K_S \to \gamma\gamma) = 8 \times 10^{-9}$, with 10% uncertainty. Using the present average [2] for BR$(K_S \to \gamma\gamma)$ we obtain the Standard Model prediction BR$(K_S \to e^+e^-) \simeq 10^{-15}$. A value significantly higher than expected would point to new physics. The best experimental limit for $BR(K_S \to e^+e^-)$ has been measured by CPLEAR [3], and it is equal to 1.4×10^{-7}, at 90% CL.

2

Here we present a new measurement of this channel, which improves on the previous result by a factor of ~ 7. This paper is organized as follows: in the next section, a brief description of the KLOE experimental setup is given; in section 3 the selection criteria for the decays of interest are summarized. Results are presented in section 4.

2 Experimental setup

The data were collected with KLOE detector at DAΦNE, the Frascati ϕ–factory. DAΦNE is an e^+e^- collider that operates at a center-of-mass energy of $\sim 1020\,$MeV, the mass of the ϕ meson. Positron and electron beams of equal energy collide at an angle of $\pi - 25\,$mrad, producing ϕ mesons with a small momentum in the horizontal plane: $p_\phi \approx 13\,$MeV$/c$. ϕ mesons decay $\sim 34\%$ of the time into nearly collinear $K^0 \bar{K}^0$ pairs. Because $J^{PC}(\phi) = 1^{--}$, the kaon pair is in an antisymmetric state, so that the final state is always $K_S K_L$. The contamination from $K_L K_L$ and $K_S K_S$ final states is neglegible. Therefore, the detection of a K_L signals the presence of a K_S of known momentum and direction, independently of its decay mode. This technique is called K_S *tagging*. The analyzed sample corresponds to an integrated luminosity of $\sim 1.3\,$fb^{-1}, yielding ~ 1.4 billion of $K_S K_L$ pairs. The KLOE detector
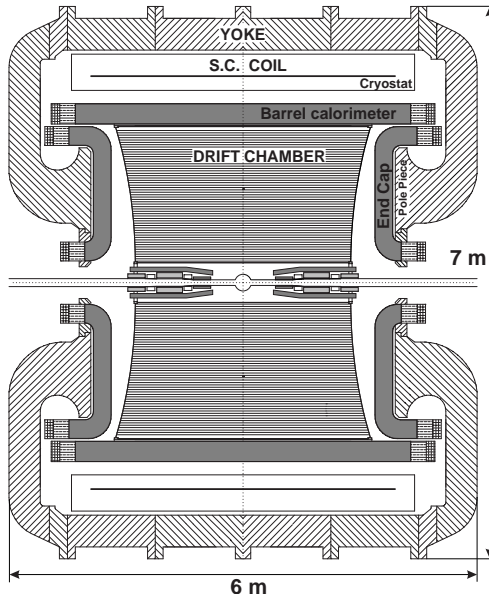

Fig. 2. Vertical cross section of the KLOE detector.

(Fig. 2) consists of a large cylindrical drift chamber (DC), surrounded by a lead/scintillating-fiber sampling calorimeter (EMC). A superconductig coil surrounding the calorimeter provides a $0.52\,$T magnetic field. The drift chamber [4], which is $4\,$m in diameter and $3.3\,$m long, has 12582 all-stereo tungsten

sense wires and 37746 aluminium field wires. The chamber shell is made of carbon-fiber/epoxy composite, and the gas used is a 90% helium, 10% isobutane mixture. These features maximize trasparency to photons and reduce $K_L \to K_S$ regeneration and multiple scattering. The DC position resolutions are $\sigma_{xy} \approx 150 \mu$m and $\sigma_z \approx 2$ mm. DC momentum resolution is $\sigma(p_\perp)/p_\perp \approx 4\%$. Vertices are reconstructed with a spatial resolution of ~ 3 mm.

The calorimeter [5] is divided into a barrel and two endcaps, contains a total of 88 modules, and covers 98% of the solid angle. The modules are read out at both ends by photomultiplier tubes. The arrival times of particles and the three-dimensional positions of the energy deposits are determined from the signals at the two ends. The read-out granularity is $\sim 4.4 \times 4.4$ cm^2; fired "cells" close in space and time are arranged into a "calorimeter cluster". For each cluster, the energy E_{cl} is the sum of the cell energies, and the time t_{cl} and the position r$_{cl}$ are calculated as energy-weighted averages over the fired cells. The energy and time resolutions are $\sigma_E/E = 5.7\%/\sqrt{E(\text{GeV})}$ and $\sigma_t = 57$ ps$/\sqrt{E(\text{GeV})} \oplus 100$ ps, respectively.

The calorimeter trigger [6] requires two local energy deposits above a threshold of 50 MeV in the barrel and 150 MeV in the endcaps. Recognition and rejection of cosmic-ray events is also performed at the trigger level: events with two energy deposits above a 30 MeV threshold in the outermost calorimeter plane are rejected as cosmic-ray events. Moreover, to reject residual cosmic rays and machine background events, an offline software filter (FILFO) exploits calorimeter and DC informations before tracks are reconstructed [7]. The trigger has a large time spread with respect to the beam crossing time. However, it is synchronized with the machine RF divided by 4, $T_{sync} \sim 10.8$ ns, with an accuracy of 50 ps. An estimate of the time of the bunch crossing producing an event is determined offline during event recostruction. This value is subtracted from the measured cluster times to obtain particle time-of-flight (TOF) measurements.

The response of the detector to the decays of interest and the various backgrounds were studied by using the KLOE Monte Carlo (MC) simulation program [7]. Changes in the machine operation and background conditions are simulated on a run-by-run basis. The most important parameters are the beam energies and the crossing angle, which are obtained from the analysis of Bhabha scattering events with $e^\pm$ polar angle above 45 degrees. The average value of the center-of-mass energy is evaluated with a precision of 30 keV for each 100 nb^{-1} of integrated luminosity. To study the background rejection, a MC sample of ϕ decays to all possible final states has been used, equivalent to an integrated luminosity of ~ 1.3 fb^{-1}. A MC sample of ~ 45000 signal events has been also produced, to measure the analysis efficiency.

3 Data analysis

3.1 K_S tagging

The identification of K_L-interaction in the EMC is used to tag the presence of K_S mesons. The mean decay lenghts of K_S and K_L are $\lambda_S \sim 0.6\,\mathrm{cm}$ and $\lambda_L \sim 350\,\mathrm{cm}$, respectively. About 50% of K_L's therefore reach the calorimeter before decaying. The K_L interaction in the calorimeter barrel (K_{crash}) is identified by requiring a cluster of energy greater than 125 MeV not associated with any track, and whose time corresponds to a velocity $\beta = r_{cl}/ct_{cl}$ compatible with the kaon velocity in the ϕ center of mass, $\beta^* \sim 0.216$, after the residual ϕ motion is considered. Cutting at $0.17 \leq \beta^* \leq 0.28$ we selected ~ 450 million K_S-tagged events (K_{crash} events in the following), which are used as a starting sample for the $K_S \to e^+e^-$ search.

3.2 Signal preselection and background normalization

$K_S \to e^+e^-$ events are selected by requiring the presence of two tracks of opposite charge with their point of closest approach to the origin inside a cylinder 4 cm in radius and 10 cm in length along the beam line. Moreover, the two tracks are required to form a vertex with position in the transverse plane $\rho < 4\,\mathrm{cm}$. The track momenta and polar angles must satisfy the fiducial cuts $120\,\mathrm{MeV}/c \leq p \leq 350\,\mathrm{MeV}/c$ and $30° \leq \theta \leq 150°$. The tracks must also reach the EMC without spiralling, and have an associated cluster. In Fig. 3, the two-track invariant mass evaluated in electron hypothesis (M_{ee}) is shown for both MC signal and background samples. A preselection cut requiring $M_{ee} > 420\,\mathrm{MeV}/c^2$ has been applied, which rejects most of $K_S \to \pi^+\pi^-$ events, for which $M_{ee} \sim 409\,\mathrm{MeV}/c^2$. The residual background has two main components: $K_S \to \pi^+\pi^-$ events, populating the low M_{ee} region, and $\phi \to \pi^+\pi^-\pi^0$ events, spreading over the whole spectrum. The $K_S \to \pi^+\pi^-$ events have such a wrong reconstructed M_{ee} because of track momentum resolution or one pion decaying into a muon. The $\phi \to \pi^+\pi^-\pi^0$ events enter the preselection because of a machine background cluster, accidentally satisfying the K_{crash} algorithm. After preselection we are left with $\sim 10^6$ events. To have a better separation between signal and background, a χ^2-like variable is defined, collecting informations from the clusters associated to the candidate electron tracks. Using the MC signal events we built likelihood functions based on:

- the sum and the difference of δt for the two tracks, where $\delta t = t_{cl} - L/\beta c$ is evaluated in electron hypothesis;
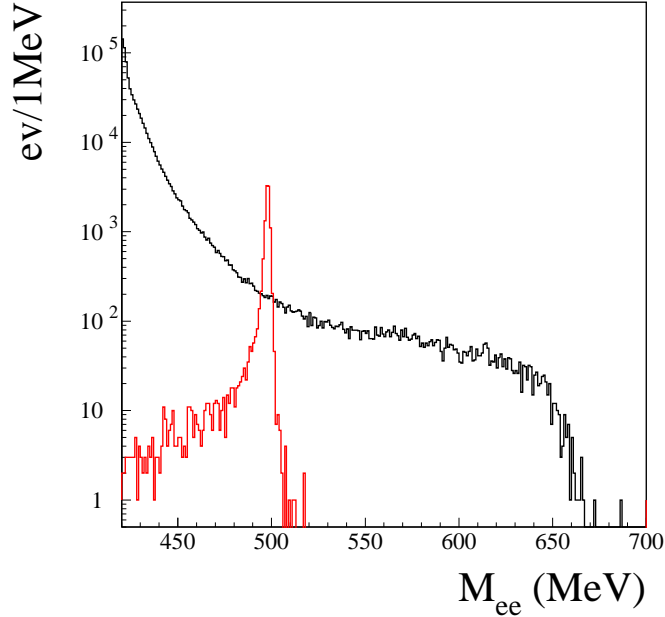- the ratio E/p between the cluster energy and the track momentum, for both

Fig. 3. Two-track invariant mass evaluated in electron hypothesis for MC signal (red) and background (black) events.

charges;
- the cluster centroid, for both charges.

In Fig. 4, the scatter plot of χ^2 versus M_{ee} is shown, for MC signal and background events. The χ^2 spectrum for background is concentrated at higher values respect to signal, since both $K_S \to \pi^+\pi^-$ and $\phi \to \pi^+\pi^-\pi^0$ events have pions in the final state. To assess the MC background normalization, two sidebands are defined in the invariant mass: $M_{ee} < 460\,\mathrm{MeV}/c^2$ (region 1 in Fig. 4), and $M_{ee} > 530\,\mathrm{MeV}/c^2$ (region 3 in Fig. 4). $K_S \to \pi^+\pi^-$ events largerly dominate on $\phi \to \pi^+\pi^-\pi^0$ in region 1, the opposite occurring in region 3. In the two sidebands, a normalization factor is evaluated for each background component, by fitting the MC spectra to data. A comparison between data and MC after the fit is shown in Fig. 5.

3.3 Background rejection

A signal box to select the $K_S \to e^+e^-$ events can be conveniently defined in the region 2 of the $M_{ee} - \chi^2$ plane (see Fig. 4); nevertheless we investigated some more independent requirements in order to reduce the background contamination as much as possible before applying the $M_{ee} - \chi^2$ selection. These cuts have been tuned on the M_{ee} sidebands, which are also used to check data-MC consistency after each step of the analysis, and they are summarized below. Charged pions from $K_S \to \pi^+\pi^-$ decay have a momentum in the K_S
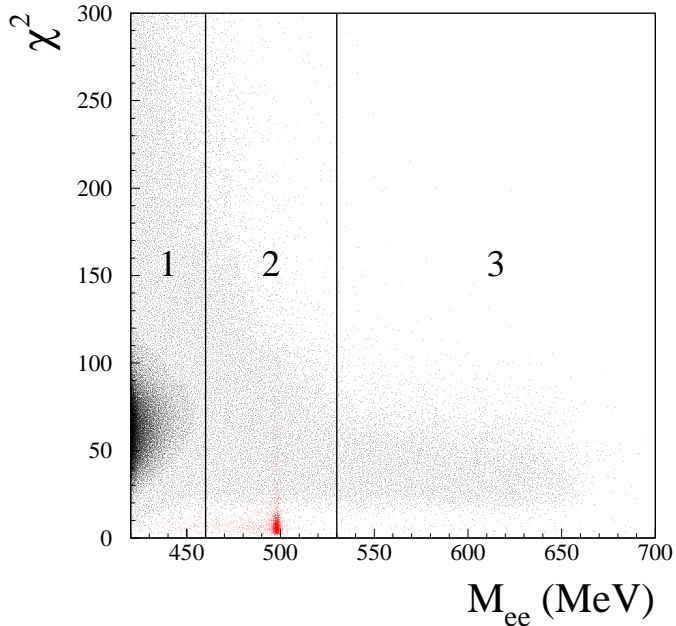
Fig. 4. Scatter plot of χ^2 versus M_{ee} for MC signal (red) and background events (black)
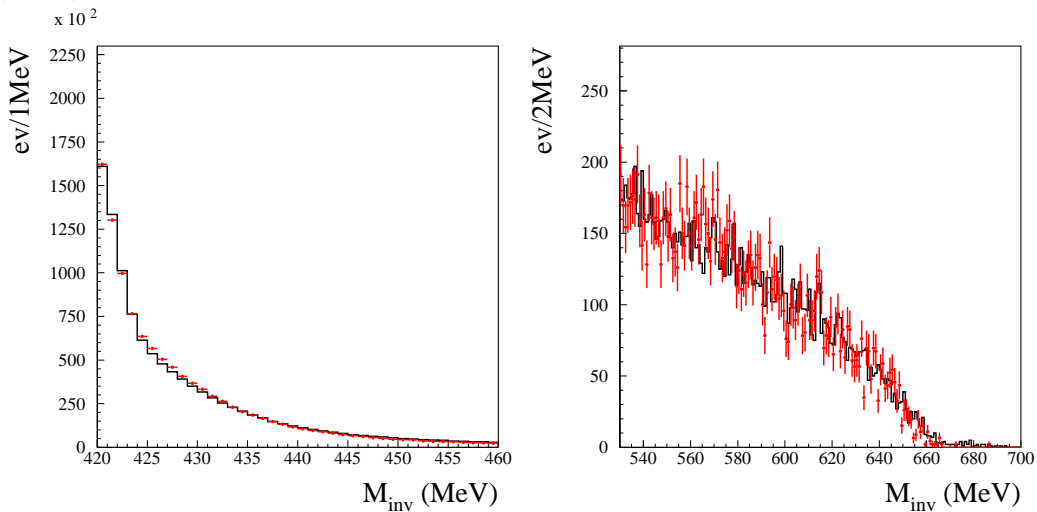

Fig. 5. Data-MC comparison for M_{ee} spectra in region 1 (left) and region 3 (right), after normalization: data are represented by the black solid line, MC by red points.

rest frame $p^*_\pi \sim 206\,\mathrm{MeV}/c$. The distribution of track momenta in the K_S rest frame, evaluated in the pion mass hypothesis, is shown in Fig. 6, for MC background in region 1, and for MC signal. For most of $K_S \to \pi^+\pi^-$ decays, at least one pion has well reconstructed momentum, so that the requirement $min(p^*_\pi(1), p^*_\pi(2)) \geq 220\,\mathrm{MeV}/c$ rejects $\sim 99.8\%$ of these events, while retaining $\sim 97\%$ of the signal. To reduce the $\phi \to \pi^+\pi^-\pi^0$ background, we can use the fact these events have two photons coming from the interaction point. The distribution of the number of prompt photons ($\delta t = t_{cl} - r_{cl}/c < 5\sigma_t$) for data and MC background in region 3, and for MC signal, is shown in
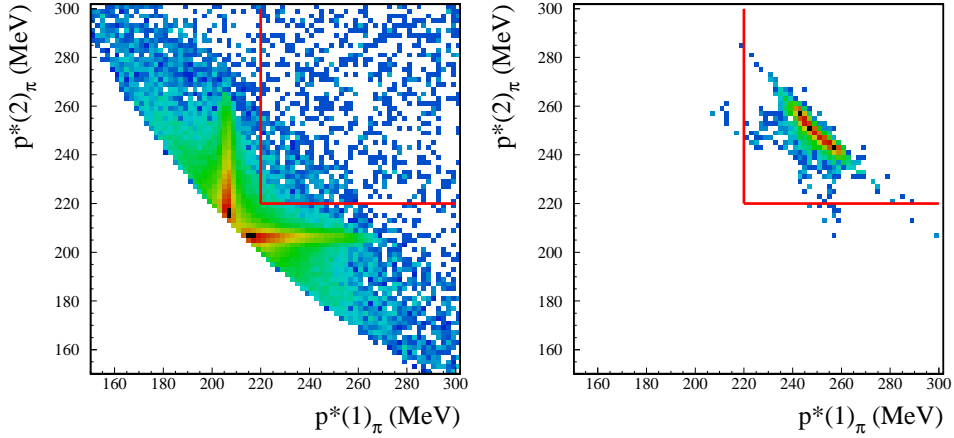
Fig. 6. Scatter plot of track momenta in the K_S rest frame (p_π^*), for MC background in region 1 (left), and for MC signal (right).

Fig. 7. We require $N_{prompt} \leq 1$, thus rejecting $\sim 65\%$ of background and only $\sim 0.1\%$ of signal events. Further rejection on $\phi \to \pi^+\pi^-\pi^0$ events is achieved
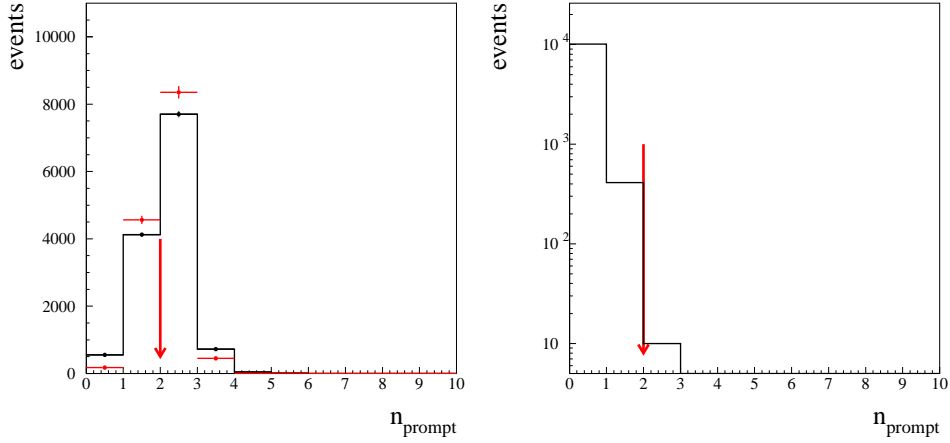

Fig. 7. Number of prompt photons (N_{prompt}) for data (black) and MC background (red) in region 3 (left), and for MC signal (right).

by cutting on the missing mass, evaluated as $M^2_{miss} = \left(\tilde{P}_\phi - \tilde{p}_+ - \tilde{p}_- \right)^2$, where $\tilde{P}_\phi$ is the ϕ four-momentum and $\tilde{p}_\pm$ are the charged track four-momenta, in pion hypothesis. Distribution of M_{miss} is shown in Fig. 8, for data and MC background in region 3, and for MC signal. We cut at $M_{miss} > 380\,\mathrm{MeV}/c^2$, rejecting almost completely the 3-pion background, peaking at the π^0 mass. A comparison between data and MC counts on the M_{ee} sidebands after each cut is shown in Tab. 1, which demonstrates the reliability of the background simulation.
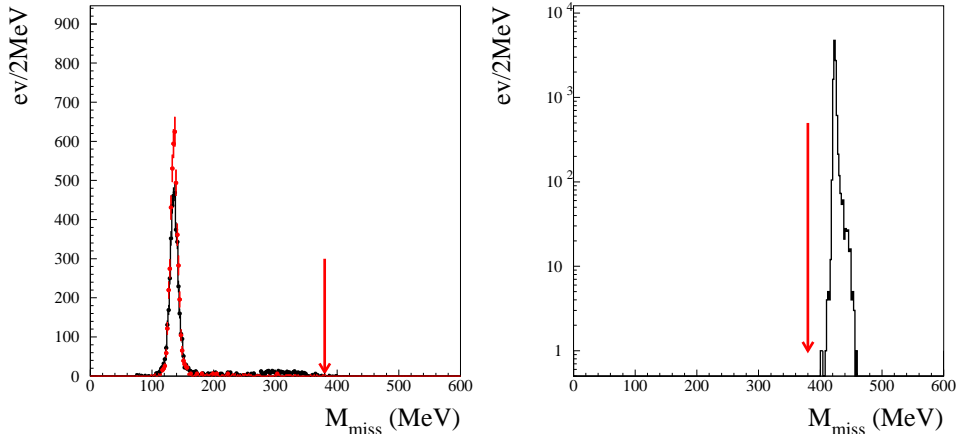
Fig. 8. Missing mass (M_{miss}) for data (black) and MC background (red) in region 3 (left), and for MC signal (right).

	Region 1			Region 3		
Cut	Data	MC bkg	Δ/σ	Data	MC bkg	Δ/σ
p_π^*	6061	6285(125)	-1.5	13144	13590(184)	-2.0
N_{prompt}	2778	2982(80)	-2.1	4672	4745(103)	-0.6
M_{miss}	1370	1407(53)	-0.6	20	5(3)	2.8

Table 1

Data and MC counts in the M_{ee} sidebands after each step of the background rejection; the relative difference between data and MC is also reported.

3.4   Signal box definition

A signal box is defined in $M_{ee} - \chi^2$ plane. To achieve the best background rejection, with maximum signal efficiency, we scan over a large set of $M_{ee} - \chi^2$ cut configurations. This optimization procedure is based on MC only, without looking at the number of observed events (N_{obs}) on data. The best configuration is:

$$\begin{cases} 492\,\text{MeV} \leq M_{ee} \leq 504\,\text{MeV} \\ \chi^2 \leq 20 \end{cases} \tag{1}$$

Applying this selection to the data sample we obtain $N_{obs} = 3$. The expected background estimated from MC is $\mu_B = 7.1 \pm 3.6$, which takes into account the MC statistics and uncertainty on the normalization factors. Using a bayesian approach [8], we evaluate the upper limit on the expected number of signal events μ_S to be $UL(\mu_S) = 4.3$, at 90% CL.

3.5   Radiative corrections

Given the chosen invariant mass selection, we actually measure the upper limit on $K_S \to e^+e^-(\gamma)$, with $E_\gamma^* < 6\,\text{MeV}$. Two processes are expected to contribute to photon emission, not interferring with each other:

- the inner bremsstrahlung photon emission, $K_S \to e^+e^- + \gamma_{IB}$;
- a $K_S \to \gamma\gamma$ decay, with one photon conversion, $K_S \to \gamma\gamma^* \to \gamma e^+e^-$.

For the first process we estimate a correction given by [9]:

$$\epsilon_{rad} = \frac{\Gamma(K_S \to e^+e^-(\gamma),\, E_\gamma^* < 6\,\text{MeV})}{\Gamma(K_S \to e^+e^-(\gamma))} = 0.8$$

The second process is strongly peaked around $M_{ee} \sim 2m_e$ [10], and a $BR(K_S \to \gamma\gamma^* \to \gamma e^+e^-) \sim 2\times10^{-16}$ is expected in our final mass window. So, our result consists in a limit on the IB emission, being insensitive, in this M_{ee} range, to the photon conversion process.

4   Results

The total selection efficiency on $K_S \to e^+e^-$ events is evaluated by MC, using the following parametrization:

$$\epsilon_{sig} = \epsilon(K_{crash}) \times \epsilon(sele|K_{crash}),$$

where $\epsilon(K_{crash})$ is the tagging efficiency, and $\epsilon(sele|K_{crash})$ is the signal selection efficiency on the sample of tagged events. The number of $K_S \to \pi^+\pi^-$ events $N_{\pi^+\pi^-}$ counted on the same sample of K_S tagged events is used as normalization, with a similar expression for the efficiency. The upper limit on $\text{BR}(K_S \to e^+e^-)$ is evaluated as follows:

$$UL(BR(K_S \to e^+e^-)) =$$
$$UL(\mu_s) \times \mathcal{R}_{tag} \times \frac{\epsilon_{\pi^+\pi^-}(sele|K_{crash})}{\epsilon_{sig}(sele|K_{crash})} \times \frac{BR(K_S \to \pi^+\pi^-)}{N_{\pi^+\pi^-}},$$

where $\mathcal{R}_{tag}$ is the tagging efficiency ratio, corresponding to a small correction due to the K_{crash} algorithm dependence on K_S decay mode. Determination of both $\mathcal{R}_{tag}$ and $\epsilon_{\pi^+\pi^-}(sele|K_{crash})$ is discussed in detail in Ref. [11]. Using as input values:

- $UL(\mu_S) = 4.3$, at 90% CL.

- $\epsilon_{sig}(sele|K_{crash}) = \underbrace{0.697}_{cuts} \times \underbrace{0.8}_{rad} = 0.558(4)$
- $\mathcal{R}_{tag} = 0.9634(1)$
- $\epsilon_{\pi^+\pi^-}(sele|K_{crash}) = 0.6102(5)$
- $N_{\pi^+\pi^-} = 148,184,688$

we obtain

$$UL(BR(K_S \rightarrow e^+e^-(\gamma))) = 2.1 \times 10^{-8}, \text{ at } 90\% \text{ CL.}$$

Systematics uncertanties, related to background normalization, are at the level of 2%. Our measurement improves by a factor of ~ 7 on the CPLEAR result [3], for the first time including radiative corrections in the evaluation of the upper limit.

References

[1] G. Ecker and A. Pich, Nucl. Phys. **B 366** (1991) 189.

[2] W.-M. Yao et al., J. Phys. J. **G 33** (2006) 1.

[3] A. Angelopoulos et al., Phys. Lett. **B 413** (1997) 232.

[4] KLOE collaboration, M. Adinolfi *et al.*, Nucl. Istrum. Meth. **A 488** (2002) 51.

[5] KLOE collaboration, M. Adinolfi *et al.*, Nucl. Istrum. Meth. **A 482** (2002) 363.

[6] KLOE collaboration, M. Adinolfi *et al.*, Nucl. Istrum. Meth. **A 492** (2002) 134.

[7] KLOE collaboration, F. Ambrosino *et al.*, Nucl. Istrum. Meth. **A 534** (2004) 403.

[8] O. Helene, Nucl. Instrum. Meth. **212** (1983) 319.

[9] C. Gatti, Eur. Phys. J. **C 45** (2005) 417.

[10] L. Bergstrom, E. Masso and P. Singer, Phys. Lett. B **131** (1983) 229.

[11] KLOE collaboration, F. Ambrosino *et al.*, Eur. Phys. J. C **48** (2006) 767